# Structure and triclustering in Ba-Al-O glass

Lawrie B. Skinner,[1,2,3] Adrian C. Barnes,[1] Philip S. Salmon,[4] Henry E. Fischer,[5] James W. E. Drewitt,[4,6] and Veijo Honkimäki[7]

[1]*H.H. Wills Physics Laboratory, University of Bristol, Tyndall Avenue, Bristol, BS8 1TL, United Kingdom*

[2]*Advanced Photon Source, Argonne National Laboratory, 9700 South Cass Avenue, Argonne, Illinois 60439, USA*

[3]*Mineral Physics Institute, Stony Brook University, Stony Brook, New York, New York 11794-2100, USA*

[4]*Department of Physics, University of Bath, Bath, BA2 7AY, United Kingdom*

[5]*Institut Laue-Langevin, 6 Rue Jules Horowitz, BP 156, F-38042, Grenoble Cedex 9, France*

[6]*CNRS-CEMHTI, University of Orleans, 1d avenue de la Recherche Scientifique, F-45071, Orléans Cedex 2, France*

[7]*European Synchrotron Radiation Facility, 6 Rue Jules Horowitz, BP 220, F-38043, Grenoble, France*

(Received 10 November 2011; published 22 February 2012)

Glass-forming ability in the $(BaO)_x(Al_2O_3)_{1-x}$ system ($0 \leqslant x \leqslant 1$) was investigated by using the containerless aerodynamic levitation and laser-heating method. The main glass-forming region was found to occur for $0.40(2) \leqslant x \leqslant 0.48(2)$, where there is insufficient oxygen to form an ideal network of corner-sharing $AlO_4$ tetrahedra in which the oxygen atoms are twofold coordinated, with another narrow glass-forming region at $x = 0.62(2)$ around the eutectic composition. The glass corresponding to $x = 0.4$ was chosen for further investigation by using both neutron and x-ray diffraction, and a detailed atomistic model was built by applying a combination of molecular dynamics and reverse Monte Carlo methods. The results show a network structure based predominantly on corner-sharing tetrahedral $AlO_4$ motifs in which triclusters ($OAl_3$ units formed by three tetrahedral Al atoms sharing a common vertex) play an integral part, with as many as 21% of the oxygen atoms involved in these configurations. The barium ions bind to an average of 7.4 O atoms, most of which are twofold-coordinated bridging oxygen atoms. The larger size of barium compared to calcium narrows the range of glass-forming compositions in alkaline-earth aluminates such that the main glass-forming range corresponds to a regime in which an oxygen-deficient Al-O network is stabilized by the formation of triclusters.

DOI: 10.1103/PhysRevB.85.064201 PACS number(s): 61.05.cp, 61.05.fg, 61.43.Bn, 61.43.Fs

## I. INTRODUCTION

Oxide glasses have many important electronic, electrochemical, and optical applications.[1–3] Several of their properties are controlled by varying the metal content where a well-known example includes the addition of rare-earth oxides to make lasers and phosphors. However, the solubility of metal oxides in network glass-forming systems such as $SiO_2$ and $GeO_2$ is often small and, in order to increase the active metal concentration, alumina ($Al_2O_3$) is often codoped with the metal oxide as in the case of calcium aluminosilicate glasses.[4] The addition of alumina to increase the metal content does, however, increase the complexity of the glass structure.

The production of pure metal aluminate glasses has been achieved for a few systems such as calcium aluminate.[5–9] Recently, containerless aerodynamic levitation and laser-heating methods, which minimize crystal formation by heterogeneous nucleation, have been employed to extend the number of glass-forming systems and/or the range of glass-forming compositions.[10–12] Such glasses avoid the complication of having to consider the effect on the structure of atoms such as Si and Ge that are present in more complex metal aluminosilicate or aluminogermanate glasses. Pure metal aluminate glasses are therefore ideal to study the characteristics of aluminate networks and, in addition, they have potential technological applications. For example, alkaline-earth aluminate glasses, which are the focus of this work, have good infrared transparency for wavelengths up to $\sim 6\ \mu$m.[13,14] This makes them suitable for window, lens, and waveguide applications where, e.g., aluminosilicate glasses have poor transmission.[6–8,15] A key driver for understanding and controlling the properties of $(MO)_x(Al_2O_3)_{1-x}$ ($0 \leqslant x \leqslant 1$) glasses, where M denotes an alkaline-earth element, is knowledge of the way in which the metal ions enter the glass structure.

A starting point for investigating the structure of these glasses is provided by inspection of the crystalline phases that are formed in systems such as calcium aluminate.[16,17] The structures are often based on corner-sharing $AlO_4$ tetrahedral units, and a model for the glass structure can be constructed on this basis.[18] Let the connectivity of each $AlO_4$ unit be classified by $Q^n$, where $n$ is the number of bridging oxygen atoms $O_B$ that are shared between neighboring Al atoms. Thus, if all of the Al atoms are fourfold coordinated by oxygen atoms and if the mean number of $O_B$ atoms per Al atom is $\langle n \rangle$, then the number of nonbridging oxygen atoms $O_{NB}$ per Al atom is $4 - \langle n \rangle$. Hence, the mean Al-$O_B$ coordination number $\bar{n}_{Al}^{O_B} = \langle n \rangle$ and the mean Al-$O_{NB}$ coordination number $\bar{n}_{Al}^{O_{NB}} = 4 - \langle n \rangle$. If each bridging oxygen is corner shared between two $AlO_4$ tetrahedra, then on average each Al atom has $4 - \langle n \rangle$ $O_{NB}$ atoms and $\langle n \rangle/2$ $O_B$ atoms such that the Al:O ratio is $1{:}4 - \langle n \rangle/2$. But, glasses of composition $(MO)_x(Al_2O_3)_{1-x}$ correspond to an Al:O:M ratio of $1{:}(3-2x)/(2-2x){:}x/(2-2x)$. Thus, $\langle n \rangle$ can be evaluated in terms of $x$ since the O:Al ratio is $4 - \langle n \rangle/2 = (3-2x)/(2-2x)$, whence

$$\langle n \rangle = (5 - 6x)/(1 - x). \tag{1}$$

From the above, the fraction of nonbridging oxygen atoms is given by $f_{O_{NB}} = (4 - \langle n \rangle)/(4 - \langle n \rangle/2) = (4x-2)/(3-2x)$ and the fraction of bridging oxygen atoms is given by $f_{O_B} = (\langle n \rangle/2)/(4 - \langle n \rangle/2) = (5-6x)/(3-2x)$. The O:Al ratio for $(MO)_x(Al_2O_3)_{1-x}$ glasses is plotted in Fig. 1 as a function of $x$.

For $x > 0.5$, the O:Al ratio is greater than two and Eq. (1) predicts that there will a mixture of bridging and nonbridging

 

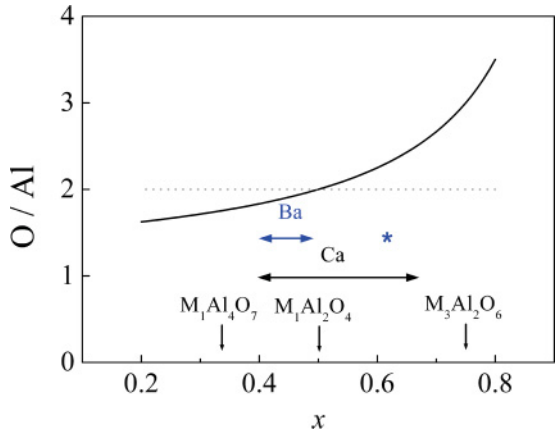


FIG. 1. (Color online) The O:Al ratio for $(MO)_x(Al_2O_3)_{1-x}$ compounds, where M denotes Ca or Ba, together with the glass-forming compositions. The O:Al ratio (solid curve) is given by $(3-2x)/(2-2x)$ (see the text) and the horizontal broken curve demarcates those compositions where the O:Al ratio is less than two ($x < 0.5$) from those where this ratio is greater than two ($x > 0.5$). The horizontal bars with arrows indicate the glass-forming regions of these systems as found by using the aerodynamic levitation and laser-heating technique. The asterisk for barium aluminate indicates an additional narrow glass-forming region at $x = 0.62(2)$ near the eutectic composition. The vertical arrows mark the compositions for which stable crystal structures occur for calcium aluminate (Refs. 16,25,30,31 and 33). Stable crystal structures for barium aluminate are also reported at these compositions with the exception of $BaAl_4O_7$ (Refs. 26,34 and 35).

oxygen atoms, consistent with the results obtained from several $^{27}$Al magic angle spinning (MAS) nuclear magnetic resonance (NMR),[13,17,19,20] diffraction,[9,21,22] spectroscopic,[16] and molecular dynamics[18,23] investigations of calcium aluminate glasses for which the glass-forming region extends well into the CaO-rich region (see Fig. 1).[5,7,8,24] A recent molecular dynamics study of $(CaO)_{0.625}(Al_2O_3)_{0.375}$ glass suggests that the nonbridging oxygen atoms in the Al-O network bind preferentially to the calcium ions.[18]

For $x = 0.5$, the O:Al ratio is exactly equal to two and Eq. (1) gives $\langle n \rangle = 4$ such that it is possible to form a network of corner-sharing $AlO_4$ tetrahedra in which all of the oxygen atoms are bridging. This scenario is observed in crystalline $CaAl_2O_4$ (Ref. 25) and $BaAl_2O_4$ (Ref. 26) and is supported by $^{27}$Al MAS NMR experiments[12,17,27] and by diffraction[21] studies on the calcium aluminate glass with $x = 0.5$. The most recent $^{27}$Al MAS NMR experiments on $CaAl_2O_4$ glass, as prepared by an aerodynamic levitation and laser-heating method, point to 96.5% of $AlO_4$ and 3.5% of $AlO_5$ units,[19] and x-ray absorption near-edge structure (XANES) spectroscopy experiments on this glass suggest that most of the $AlO_4$ units form $Q^4$ sites.[28]

For $x < 0.5$, however, the O:Al ratio is less than two and the model of corner-sharing $AlO_4$ units with twofold-coordinated oxygen atoms, which leads to Eq. (1), must break down. For this composition range, a comparison with calcium aluminate crystal structures suggests that either (i) three $AlO_4$ units share an oxygen atom at a vertex to form a so-called tricluster ($AlO_3$ unit) (Ref. 29) as in crystalline $CaAl_4O_7$ ($x = 1/3$) (Refs. 30 and 31) or (ii) $AlO_5$ and $AlO_6$ units form as in crystalline $CaAl_{12}O_{19}$ ($x = 1/7$).[32] Fivefold- and sixfold-coordinated Al atoms have been observed in $^{27}$Al MAS NMR experiments on calcium aluminate glasses with $x \leqslant 0.4$ as formed by a rapid (splat) quenching method.[17] Another possibility is the formation of edge- or face-sharing $AlO_4$ tetrahedra, although these are not generally observed in crystalline calcium aluminates.[16]

As indicated by the above discussion, the majority of work on alkaline-earth aluminate glasses has been on the calcium-based system. The object of this work is to extend these studies to the barium aluminate system to explore the effect of the larger size of the $M^{2+}$ ion on the glass properties. Although these glasses have been prepared as small spheres of 100-$\mu$m diameter,[36] and results for barium aluminate glasses such as BaO-ZnO-$Al_2O_3$ containing additional metal oxides have been published,[37,38] it is only recently that a barium aluminate glass has been made in bulk by using the aerodynamic levitation and laser-heating method.[39] Here, we use this method to investigate the glass-forming region in the barium aluminate system and compare the results with those previously obtained for the calcium aluminate system.[24] In the case of barium aluminate, we find that glass formation occurs in the range $0.40(2) \leqslant x \leqslant 0.48(2)$ where the O:Al ratio $\lesssim 2$, and that there is another narrow region of glass formation at $x = 0.62(2)$ around the eutectic composition.[34] Thus, the majority of barium aluminate glasses form in a composition range where there are insufficient oxygen atoms to form a network of corner-sharing $AlO_4$ tetrahedra. This formation of an oxygen-deficient network is unusual and, in consequence, we made a detailed structural investigation of glassy $(BaO)_{0.4}(Al_2O_3)_{0.6}$ (or $Ba_2Al_6O_{11}$) using x-ray and neutron diffraction. A detailed picture of the glass structure was then obtained by using a modeling technique in which the atomistic configurations produced from a molecular dynamics (MD) simulation were refined by reference to the diffraction data by using the reverse Monte Carlo (RMC) method.[40] We find that oxygen triclusters form an integral part of a glass network made predominantly from corner-sharing $AlO_4$ tetrahedra in which the $Ba^{2+}$ ions bind preferentially to twofold-coordinated oxygen atoms.

The paper is organized as follows. The essential theory for the neutron and x-ray diffraction experiments is given in Sec. II. The experimental methods are described in Sec. III, and the molecular dynamics and RMC procedures are described in Sec. IV. The diffraction and modeling results are presented in Sec. V and are discussed in Sec. VI. Conclusions are drawn in Sec. VII.

## II. THEORY

In a neutron or x-ray diffraction experiment on $(BaO)_{0.4}(Al_2O_3)_{0.6}$ glass, the coherent scattered intensity can be represented by the total structure factor $S(Q)$ defined by[41]

$$S(Q) - 1 = \frac{1}{|\langle w(Q) \rangle|^2} \times \sum_{\alpha} \sum_{\beta} c_\alpha c_\beta w_\alpha^*(Q) w_\beta(Q) [S_{\alpha\beta}(Q) - 1], \quad (2)$$

TABLE I. The coherent neutron scattering lengths $b_\alpha$ together with the total bound scattering cross section $\sigma_{\text{scat},\alpha}$ and the absorption cross section $\sigma_{\text{abs},\alpha}$ at an incident neutron wavelength of 1.798 Å for Ba, Al, and O as taken from Ref. 42.

| Atom | $b_\alpha$ (fm) | $\sigma_{\text{scat},\alpha}$ (barn) | $\sigma_{\text{abs},\alpha}$ (barn) |
|---|---|---|---|
| Ba | 5.07(3) | 3.38(10) | 1.1(1) |
| Al | 3.449(5) | 1.503(4) | 0.231(3) |
| O | 5.805(4) | 4.232(6) | 0.00019(2) |

where $c_\alpha$ and $w_\alpha(Q)$ represent the atomic fraction and scattering length (or form factor) of chemical species $\alpha$, respectively, and $Q$ denotes the magnitude of the scattering vector. In Eq. (2), $\langle w(Q)\rangle = \sum_\alpha c_\alpha w_\alpha(Q)$ is the mean scattering length and $S_{\alpha\beta}(Q)$ denotes a Faber-Ziman partial structure factor. For the case of neutron diffraction, the total structure factor is denoted by $S_{\text{N}}(Q)$ and $w_\alpha(Q)$ corresponds to the coherent neutron scattering length $b_\alpha$, which is independent of $Q$. For the case of x-ray diffraction, the total structure factor is denoted by $S_{\text{X}}(Q)$ and $w_\alpha(Q) = f_\alpha(Q) + f'_\alpha(E_0) + if''_\alpha(E_0)$ where $f_\alpha(Q)$ is the form factor for chemical species $\alpha$, while $f'_\alpha(E_0)$ and $f''_\alpha(E_0)$ are the real and imaginary parts of the anomalous term for chemical species $\alpha$, respectively. The latter depend on the incident energy $E_0$ of the photons. The coherent neutron scattering lengths were taken from Ref. 42 and are listed in Table I. The x-ray form factors were taken from Ref. 43 and the anomalous terms were calculated using the FPRIME program.[44] The relative weighting factors given to the partial structure factors in $S_{\text{N}}(Q)$ and in $S_{\text{X}}(Q)$ at $Q = 0$ for $(BaO)_{0.4}(Al_2O_3)_{0.6}$ glass are shown in Fig. 2.

The total pair distribution function $G(r)$ is obtained from the Fourier transform relation[41]

$$G(r) - 1 = \frac{1}{2\pi^2\rho r}\int_0^\infty Q[S(Q) - 1]\sin(Qr)dQ, \quad (3)$$

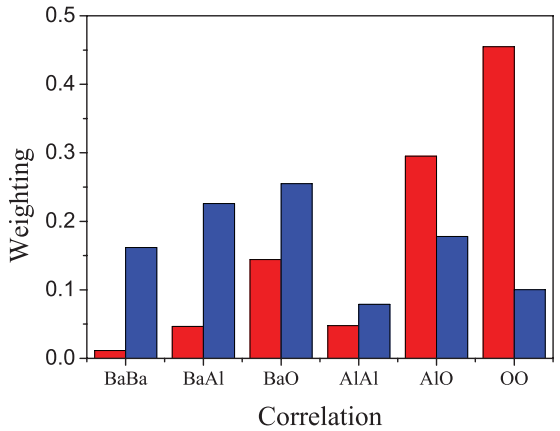


FIG. 2. (Color online) The relative weighting factors given to the partial structure factors for neutron versus x-ray diffraction experiments on $(BaO)_{0.4}(Al_2O_3)_{0.6}$ glass as calculated by using Eq. (2). The neutron and x-ray data sets are represented by the light (red) and dark (blue) histograms, respectively. The x-ray values were calculated for $Q = 0$.

where $\rho$ is the atomic number density of the material. For the case of neutron diffraction, the total pair distribution function is denoted by $G_{\text{N}}(r)$ and is a linear combination of the partial pair distribution functions $g_{\alpha\beta}(r)$, which are given the same relative weighting factors as the partial structure factors in the expression for $S_{\text{N}}(Q)$ [Eq. (2)]. For the case of x-ray diffraction, the total pair distribution function is denoted by $G_{\text{X}}(r)$ and the $Q$-dependent scattering lengths $w_\alpha(Q)$ add a complication. Each $g_{\alpha\beta}(r)$ term in $G_{\text{X}}(r)$ is convoluted with a modification function $M_{\alpha\beta}(r)$, which is related to the Fourier transform of the $Q$-dependent weighting factor for the corresponding $S_{\alpha\beta}(Q)$ function as given in Eq. (2). A detailed discussion of the effect of these modification functions on the real-space pair distribution functions is given by Zeidler *et al.*,[45] and a consequence is that the peak shapes will be significantly different from those observed by neutron diffraction. However, for the case when $G_{\text{X}}(r)$ has a clearly identifiable and isolated peak corresponding to a single partial pair distribution function $g_{\alpha\beta}(r)$, it is possible to reproduce an identical peak to that observed in a neutron diffraction measurement by Fourier transforming a *modified* $S_{\text{X}}(Q)$ function in which the relevant partial structure factor is given a $Q$-independent weighting factor.[45] The mean coordination number of atoms of type $\beta$, contained in a volume defined by two concentric spheres of radii $r_i$ and $r_j$ centered on an atom of type $\alpha$, is given by

$$\bar{n}_\alpha^\beta = 4\pi\,\rho\,c_\beta\int_{r_i}^{r_j} dr\,r^2 g_{\alpha\beta}(r). \quad (4)$$

To emphasize the features describing the structure at larger $r$ values, it is convenient to consider the density function which, for neutron diffraction, is defined by

$$D_{\text{N}}(r) = 4\pi\rho r[G_{\text{N}}(r) - 1] = \sum_\alpha\sum_\beta \frac{c_\alpha c_\beta b_\alpha b_\beta}{|\langle b\rangle|^2} d_{\alpha\beta}(r), \quad (5)$$

where $d_{\alpha\beta}(r) = 4\pi\rho\,r[g_{\alpha\beta}(r) - 1]$ and $\langle b\rangle = c_\alpha b_\alpha + c_\beta b_\beta$ is the mean coherent neutron scattering length.

## III. EXPERIMENTAL METHOD

### A. Sample preparation

Samples of BaO-$Al_2O_3$ glass were made by aerodynamic levitation and laser heating[10] using high-purity alumina (99.99%, Sigma Aldrich) and barium carbonate (>99%, Aldrich). Each powder was heated to 1000 °C in air for 24 h, ground, and then reheated to 1000 °C for a further 12 h to eliminate any water and $CO_2$ content. The resulting $Al_2O_3$ and BaO powders were mixed in equimolar quantities and fused by laser heating on a water-cooled copper hearth.[46] The fused powders were then levitated on a conical nozzle aerodynamic levitation and laser-heating system (supplied by Containerless Research Incorporated, Evanston, IL, USA) using a 1:4 oxygen:argon mixture as the levitation gas stream. The samples were heated to just above their melting point, held for 30 s to ensure complete mixing, and then rapidly quenched by abruptly cutting the heating laser power.[39] For samples of 2 mm diameter, this corresponds to a cooling rate of $\simeq$300 K $s^{-1}$at 2000 K.

It was found from gravimetric analysis that some loss of sample mass occurred during this procedure such that the original equimolar composition was not preserved. This loss was attributed to an evaporation of BaO during synthesis owing to its comparatively low boiling point ($\sim$2000 °C).[47] The precise sample composition, after synthesis, was verified by wavelength dispersive microprobe analysis and was found to be $x = 0.40(2)$, corresponding to $(BaO)_{0.4}(Al_2O_3)_{0.6}$. Self-consistency checks were also made during the x-ray and neutron diffraction data analysis procedures to ensure that this composition gave the correct sample attenuation factors. The atomic number density of the samples was measured to be 0.0682(8) Å$^{-3}$ using Archimedes principle and submersion in toluene. The calibration was confirmed by using perfect stainless-steel ball bearings.

Glass formation in both the barium aluminate and calcium aluminate systems was also investigated. Spherical samples of 2 mm diameter were again prepared by melting the starting powders in the levitation apparatus, equilibrating for 30 s, and rapidly quenching by abruptly cutting the laser power. The cooling rate for these samples was $\simeq$300 K s$^{-1}$ at 2000 K. Evidence for sample recrystallization was obtained from (i) the appearance of a recalescence signature in a pyrometer trace of the sample temperature after the onset of supercooling and (ii) by visual inspection of the sample at room temperature, where a turbid appearance indicates the formation of crystallites.[39,48] The Ba-containing samples lost mass on preparation and their composition was determined using the methodology described above. The Ca-containing glasses showed no mass loss on fabrication and the sample compositions were assumed to be those defined by the masses of the initial powders.

Figure 1 shows the glass-forming regions that were found for the $(MO)_x(Al_2O_3)_{1-x}$ (M = Ba or Ca) systems and also shows the O:Al ratio corresponding to the different $x$ values. Our results confirm the glass-forming region for the composition range $0.4 \lesssim x \lesssim 0.67$ observed previously for calcium aluminate by using the containerless aerodynamic and laser-heating method[24] and show that this region is much wider than for the barium aluminate analog for which $0.40(2) \leqslant x \leqslant 0.48(2)$. An additional very narrow glass-forming region was also located for barium aluminate at $x = 0.62(2)$, around the reported eutectic in the phase diagram at $x = 0.658$–$0.684$.[34]

### B. Diffraction measurements

Neutron and x-ray diffraction measurements were carried out under ambient conditions using the instruments D4c (Ref. 49) and ID15B at the Institut Laue-Langevin (ILL) in Grenoble and the European Synchrotron Radiation Facility (ESRF) in Grenoble, respectively. For the neutron diffraction experiment, a large number ($\gtrsim$50) of glass spheres of identical composition were fabricated and placed into a cylindrical vanadium can of 4.8 mm inner diameter and 0.1 mm wall thickness. An incident neutron wavelength of $\lambda = 0.4965(1)$ Å was used, giving a scattering vector range of $0.4 \leqslant Q \leqslant 23.5$ Å$^{-1}$. The diffraction data were corrected[41] for background and container scattering, self-attenuation, multiple scattering, and inelasticity (Placzek) effects to give the total structure factor $S_N(Q)$ defined by Eq. (2). The x-ray diffraction experiment was carried out using transmission geometry at a high incident photon energy of 88.76 keV corresponding to a wavelength $\lambda = 0.1394(2)$ Å. The scattering vector range was $0.5 \leqslant Q \leqslant 17.8$ Å$^{-1}$. In order to minimize the sample self-attenuation and multiple scattering corrections, the sample was polished into a thin disk of thickness $<1$ mm and was mounted in a thin-walled kapton container. The data sets were collected as two-dimensional (2D) images using a MAR345 image plate detector and were corrected for polarization and geometric effects[50] using the FIT2D software.[51] The diffraction data were then corrected[41] for background and container scattering, Compton scattering, fluorescence, and self-attenuation to give the total structure factor $S_X(Q)$ defined by Eq. (2).

## IV. MODELING METHODS

### A. Molecular dynamics simulation

Molecular dynamics simulations were carried out using the DLPOLY2 package[52,53] with modified Buckingham interatomic pair potentials of the form

$$V_{\alpha\beta}(r) = Z_\alpha Z_\beta e^2/r + A_{\alpha\beta}\exp(-B_{\alpha\beta}r) - C_{\alpha\beta}/r^6. \quad (6)$$

In this equation, $Z_\alpha e$ is the charge on species $\alpha$, $e$ is the elementary charge, $A_{\alpha\beta}$ and $B_{\alpha\beta}$ control the magnitude and decay of the short-ranged repulsive part of the potential, and $C_{\alpha\beta}$ controls the magnitude of the van der Waals term. The values of the coefficients used for the Ba-O, Al-O, and O-O pair potentials were taken from Ref. 54 and are listed in Table II. The Ba-Ba, Al-Al, and Ba-Al interactions were modeled using only the Coulomb term in Eq. (6). The simulations were carried out using an $NVT$ ensemble with 1499 atoms (157 Ba, 474 Al, 868 O) and a cubic cell of length 28 Å corresponding to an atomic number density $\rho = 0.0682$ Å$^{-3}$. The simulations were started at 4000 K from an initial random configuration of particles subject to minimum initial nearest-neighbor distances of 1.3 Å for the Al-O pairs and 2 Å for the other pairs of particles. The total simulation time was 200 ps taken in 50-ps steps at 4000, 1800, 1500, and 298 K, respectively. The final configuration at 298 K was refined by reference to diffraction data by the using the RMC method.

### B. Reverse Monte Carlo refinement

The MD simulations are based on simple pair potentials and are not, therefore, expected to give an accurate description of a glass structure when three-body forces are important. They do, however, give a basic description of the chemical and topological ordering in the glass, as subjected to charge

TABLE II. The coefficients used for the interatomic pair potentials in the MD simulation [Eq. (6)] (Ref. 54). The Ba-Ba, Al-Al, and Ba-Al pair potentials were taken to be purely Coulombic such that $A_{\alpha\beta} = C_{\alpha\beta} = 0$.

| | $Z_\alpha$ | $Z_\beta$ | $A_{\alpha\beta}$ (eV) | $B_{\alpha\beta}$ (Å$^{-1}$) | $C_{\alpha\beta}$ (eV Å$^{-6}$) |
|---|---|---|---|---|---|
| Ba-O | +2 | −2 | 4818 | 3.261 | 0 |
| Al-O | +3 | −2 | 2409 | 3.775 | 0 |
| O-O | −2 | −2 | 25.41 | 1.442 | 32.32 |

TABLE III. The distances of closest approach for pairs of atoms in the MD simulation of $(BaO)_{0.4}(Al_2O_3)_{0.6}$ glass, as obtained from the minimum values of $r$ for which $g_{\alpha\beta}(r) > 0$, compared to the minimum cutoff distances used in the RMC refinement of this glass structure and to the shortest interatomic distances in crystalline $BaAl_2O_4$ (Ref. 26). All distances are given in units of Å.

| | Ba-Ba | Ba-Al | Ba-O | Al-Al | Al-O | O-O |
|---|---|---|---|---|---|---|
| MD glass | 3.1 | 2.9 | 2.4 | 2.4 | 1.5 | 2.0 |
| RMC glass | 3.1 | 2.8 | 2.4 | 2.4 | 1.4 | 2.1 |
| $BaAl_2O_4$ cryst | 4.41 | 3.48 | 2.75 | 3.18 | 1.74 | 2.56 |

neutrality and atomic number density constraints, and thus provide an atomistic model, which can then be refined with reference to our x-ray and neutron diffraction results by using the RMC method.[40] In this procedure, the reciprocal space data sets were fitted.

In order to maintain the basic configuration obtained from the MD simulation, the step size of the atomic movements in the RMC procedure was restricted to 0.05 Å such that no atom moved more than 1 Å from its original starting position. The overall average of the root-mean-square displacements of the atoms in the procedure was 0.4 Å. The distances of minimum approach between the various pairs of atoms in the RMC refinement were constrained in accordance with the parameters given in Table III, where the shortest nearest-neighbor interatomic distances in crystalline $BaAl_2O_4$ (Ref. 26) and in the MD simulations of the $(BaO)_{0.4}(Al_2O_3)_{0.6}$ glass are also listed.

Several RMC refinement strategies were employed. In the first (RMC-I), no coordination number constraints were applied. In the second (RMC-II), the barium atoms were fixed at the positions obtained from the MD simulation, and only the aluminium and oxygen atoms were allowed to move. In the third (RMC-III), the Al-O coordination number was constrained to be 4 for all of the Al atoms in the model, corresponding to a network based on 100% $AlO_4$ tetrahedral motifs.

## V. RESULTS

### A. Diffraction results

The measured neutron and x-ray total structure factors $S_N(Q)$ and $S_X(Q)$ show a significant contrast (Fig. 3), in accordance with the different relative weighting factors given to the partial structure factors (Fig. 2), where the neutron diffraction data are more sensitive to the O-O and Al-O correlations and the x-ray data are more sensitive to the Ba atom correlations. The diffraction patterns show no Bragg peaks, i.e., although the sample composition corresponds to an edge of the main glass-forming region, the glass is free from crystalline inclusions.

The total pair distribution functions $G_N(r)$ and $G_X(r)$ are shown in Fig. 4. The first peak at 1.75(2) or 1.77(2) Å is identified with Al-O correlations and gives a coordination number $\bar{n}^O_{Al}$ of 4.0(2) or 4.0(4), respectively, where the procedure outlined in Sec. II was used to extract $\bar{n}^O_{Al}$ from $G_X(r)$. The small peak in $G_N(r)$ at $\simeq$2.1 Å is a Fourier transform artifact arising from the relatively small maximum value

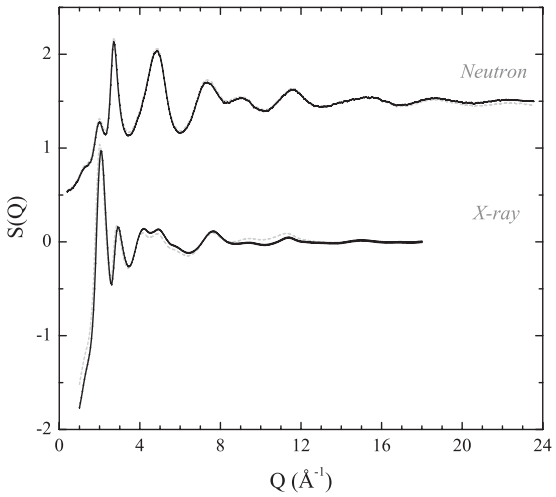


FIG. 3. The measured neutron and x-ray total structure factors $S_N(Q)$ and $S_X(Q)$. The solid dark (black) curves show the measured functions and the broken light (gray) curves show the back Fourier transforms of the corresponding $G_N(r)$ and $G_X(r)$ functions given by the broken light (gray) curves in Fig. 4 after the unphysical oscillations at $r \leqslant 1.45$ Å have been set to the calculated limit for $G_N(r = 0)$ or $G_X(r = 0)$. The maximum value $Q_{max}$ is 23.5 Å$^{-1}$ for $S_N(Q)$ and 17.8 Å$^{-1}$ for $S_X(Q)$. The data sets have been shifted vertically for clarity of presentation.

$Q_{max} = 23.5$ Å$^{-1}$, which truncates the high-$Q$ oscillations in $S_N(Q)$ before they have fully decayed. As shown in Fig. 4, the Fourier transform artifacts are reduced by application of a Lorch[55] modification function, but at the expense of a loss in resolution of the first few peaks in $r$ space.

The first peak positions and coordination numbers in $G_N(r)$ and $G_X(r)$ point to a network built predominantly from $AlO_4$ tetrahedra. The first peak does not show a shoulder on its

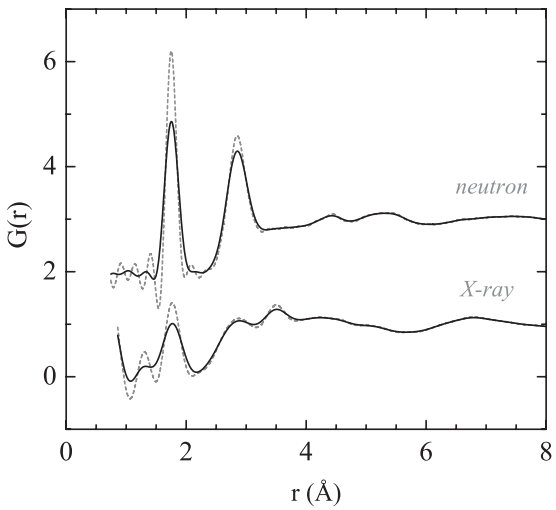


FIG. 4. The total pair distribution functions $G_N(r)$ and $G_X(r)$ obtained by Fourier transforming the data sets shown by the solid dark (black) curves in Fig. 3 before [broken light (gray) curves] and after [solid dark (black) curves] the application of a Lorch modification function (Ref. 55). The data sets have been shifted vertically, and the Fourier transform artifacts for $r < 1.45$ Å have been omitted, for clarity of presentation.

high-$r$ side in the range 1.83–1.91 Å, which corresponds to typical bond lengths in $AlO_5$ and $AlO_6$ structural motifs. It would, nevertheless, be advantageous to further explore this possibility by extending $Q_{max}$ for the diffraction experiments to give better resolution of the $r$-space functions.[9,56] The second peak in $G_N(r)$ or $G_X(r)$ comprises overlapping pair distribution functions where the nearest-neighbor O-O and Ba-O distances are expected to be 2.81–2.99 and 2.86–2.87 Å, respectively.[26] A peak at ∼3.5 Å occurs in $G_X(r)$ but not in $G_N(r)$ and, by comparison, with the crystal structure of $BaAl_2O_4$,[26] may arise from Ba-Al correlations.

### B. Molecular dynamics

Figure 5 compares the measured $S_N(Q)$ and $S_X(Q)$ functions with those predicted from the MD simulations. There is broad overall agreement between experiment and simulation, which suggests that the MD results act as a good starting point for understanding the glass structure. For both the neutron and x-ray data sets, there is a small phase shift at high $Q$, which is indicative of an error in the predicted Al-O distance. The relative fractions of $AlO_4$ and $AlO_5$ units are found to be 86.7% and 13.3%, respectively, with a few $AlO_3$ and $AlO_6$ units also present. Of the different Al-centered polyhedra, the majority are corner sharing (88.9%), while the remainder are edge sharing (11.0%), as determined by using an Al-O cutoff distance of 2.1 Å. The $AlO_4$-$AlO_4$ connections are predominantly corner sharing (∼97%), the $AlO_4$-$AlO_5$ connections show a smaller corner-sharing tendency (∼75%), whereas the $AlO_5$-$AlO_5$ connections show a preference for edge sharing (∼59%). The MD results therefore predict corner-sharing $AlO_4$ tetrahedra to be the predominant network forming structural motifs. The oxygen atoms are mostly twofold (∼71%) or threefold (∼27%) coordinated to Al atoms and, of the latter, ∼35% are bound to Al atoms in $AlO_4$ units, i.e., they are in tricluster conformations.

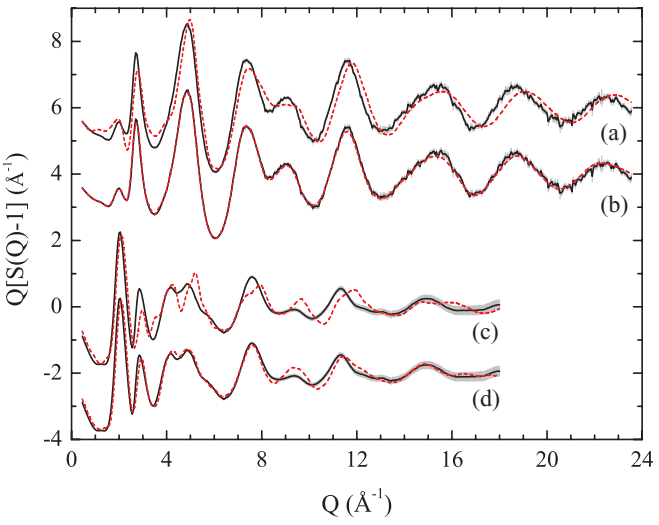


FIG. 5. (Color online) A comparison between the measured and modeled functions $Q[S_N(Q)-1]$ and $Q[S_X(Q)-1]$ for $(BaO)_{0.4}(Al_2O_3)_{0.6}$ glass. The solid dark (black) curves with gray vertical lines show the measured data sets and associated statistical errors, respectively, while the broken light (red) curves show the results obtained from the models. $Q[S_N(Q)-1]$ is compared with the results obtained from (a) the MD simulation and (b) the RMC-I refinement of the MD model in which no coordination number constraints were applied. $Q[S_X(Q)-1]$ is compared with the results obtained from (c) the MD simulation and (d) the RMC-I refinement. In (a), (b), and (d), the data sets have been shifted vertically for clarity of presentation.

There is a broad range of Ba-O coordination numbers in the MD model, corresponding to a broad distribution of Ba-centered polyhedra. In consequence, the first Ba-O coordination shell is poorly defined in that the Ba-O partial pair distribution function does not go to zero on the high-$r$ side of the first peak (Fig. 6). The coordination number $\bar{n}^{O}_{Ba}$ evaluated by using Eq. (4) is 7.0 or 9.2 for large-$r$ cutoff distances of 3.4 or 3.8 Å, respectively. A large-$r$ tail to the first M-O peak is also seen in calcium aluminate glasses[18,23,57] and in the calcium aluminosilicate glass $(CaO)_{0.48}(SiO_2)_{0.49}(Al_2O_3)_{0.03}$.[58,59]

### C. RMC refinements

The RMC-I refinement of the MD data, in which no coordination number constraints were applied, converged to give a good fit to the diffraction data without the need for any large movement of the atoms from their initial positions. This indicates that a representative glass structure can be obtained from a true refinement of the atomic configurations found from the MD simulation rather than from a complete rearrangement of the atomic coordinates. The RMC-I fits to the diffraction data, as obtained by averaging over several independent configurations, are shown in Fig. 5, and a comparison between the MD and RMC-I partial structure factors $S_{\alpha\beta}(Q)$ and partial pair density functions $d_{\alpha\beta}(r)$ is made in Fig. 6.

On applying the RMC-I method to the MD model, there is an increase in position of the first Al-O peak from 1.72 to 1.77 Å and a small alteration in the region around 3–5 Å. The relative fraction of $AlO_4$ units increases to 98.5% while a few $AlO_3$ and $AlO_5$ units are also present. Of the different Al-centered polyhedra, 94.8% are corner sharing and 5.2% are edge sharing (as found for a cutoff distance of 2.1 Å), and the latter tend to be associated with nontetrahedral motifs. The $AlO_4$-$AlO_4$ connections are predominantly corner sharing (∼97%). The partial pair density functions involving the barium atoms show little change, apart from $d_{BaO}(r)$ where the first peak at 2.81 Å becomes a broad peak at 2.86 Å. The Ba-O coordination number is largely unchanged at 7.4 or 9.5 for large-$r$ cutoff distances of 3.4 or 3.8 Å, respectively. The most notable changes that occur on refining the MD model are observed in the Al-Al correlation functions where the oscillations in $S_{AlAl}(Q)$ become more heavily damped and the first feature in $d_{AlAl}(r)$, which shows peaks at ≃2.8 and ≃3.2 Å, is broadened. It should be noted, however, that the Al-Al pair correlations receive a small weighting factor in both the neutron and x-ray diffraction data sets (Fig. 2). The nature of the Al-Al correlations in the barium aluminate glass is discussed in more detail in Sec. VI A.

The MD model was also refined (RMC-II) by fixing the Ba atom positions and allowing only the Al and O atoms to move. This procedure did not change the quality of the fit to the diffraction data and led to a relative fraction of $AlO_4$ tetrahedra (98.5%) that is comparable to the results obtained from RMC-I. In the third refinement procedure (RMC-III), the

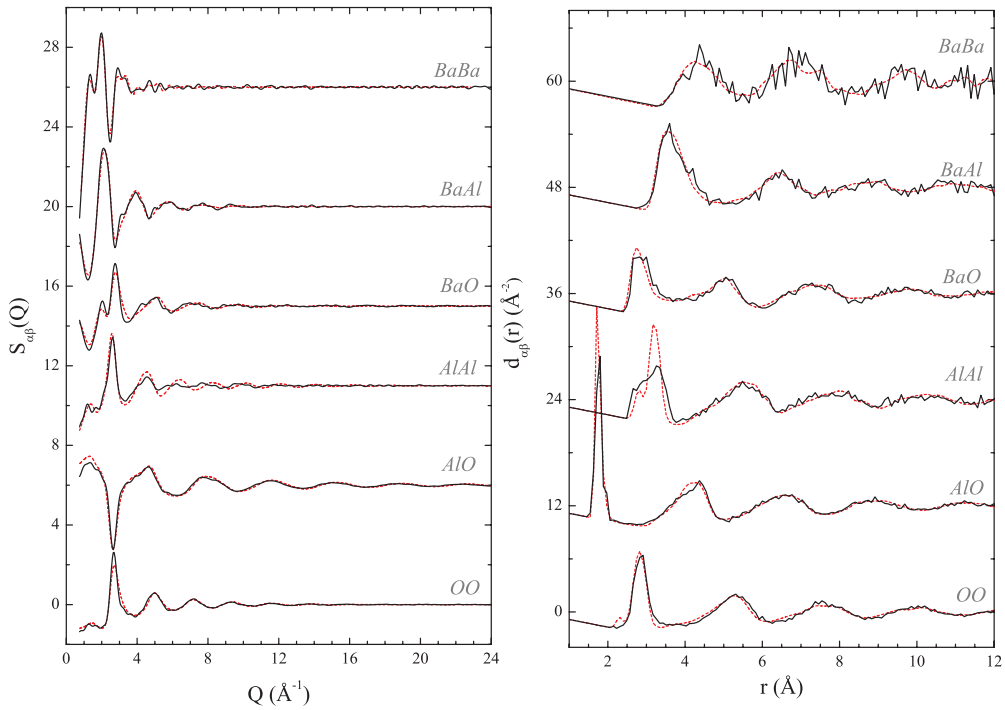


FIG. 6. (Color online) The partial structure factors $S_{\alpha\beta}(Q)$ and partial pair density functions $d_{\alpha\beta}(r)$ for $(BaO)_{0.4}(Al_2O_3)_{0.6}$ glass as obtained from the MD simulation [broken (red) curves] and from the RMC-I refinement of the MD model in which no coordination number constraints were applied [solid (black) curves].

model was constrained so that 100% of the Al atoms were in $AlO_4$ tetrahedra. Enforcing this constraint made no significant difference to the quality of the fits to the diffraction data. Additionally, for all of the RMC models, the ratio $r_{OO}/r_{AlO}$ for the first peak positions in $g_{OO}(r)$ and $g_{AlO}(r)$ is found to be 1.63(1), close to the ratio $\sqrt{8/3} = 1.633$ expected for a perfect $AlO_4$ tetrahedron. Thus, all of the models point to a glass network constructed predominantly from corner-sharing $AlO_4$ tetrahedral motifs. It would be useful to test this expectation by using $^{27}$Al MAS NMR.[17,19,20,56]

## VI. DISCUSSION

### A. Network glass structure

In the case of most tetrahedral glass-forming systems with a 2:1 stoichiometry, such as $SiO_2$, $GeO_2$, and $GeSe_2$, the tetrahedra are corner shared ($SiO_2$, $GeO_2$) or corner and edge shared ($GeSe_2$).[60–63] However, the glass studied in this work is oxygen deficient in the sense that the O:Al ratio is well below the value of 2 required to produce a perfectly connected tetrahedral network in which the O and Al atoms are twofold and fourfold coordinated, respectively.[64] In the case of an ideal network built from corner-sharing $AlO_4$ tetrahedra, this oxygen deficiency *requires* an oxygen coordination number greater than two, i.e., the existence of oxygen triclusters.[29–31,65,66]

The fraction of oxygen atoms forming triclusters in $(BaO)_x(Al_2O_3)_{1-x}$ glass can be estimated by introducing a model in which the $Ba^{2+}$ ions fit into a network of $AlO_4$ tetrahedra that are connected such that none of the oxygen atoms in the network are isolated (nonbonded) or nonbridging (i.e., not shared with a neighboring tetrahedron). For every $2(1-x)$ Al atoms, there are $(3-2x)$ O atoms so that we can think of the Al and O atoms as forming a network in which the atomic fraction of Al atoms is given by

$$c_{Al} = 2(1-x)/(5-4x) \tag{7}$$

and the atomic fraction of O atoms is given by

$$c_O = (3-2x)/(5-4x). \tag{8}$$

If the total number of oxygen atoms in the network is given by $N_O = N_{2O} + N_{3O}$, where $N_{2O}$ and $N_{3O}$ are the number of twofold- and threefold-coordinated oxygen atoms, respectively, then it follows that

$$\bar{n}_O^{Al} = \frac{c_{Al}}{c_O}\bar{n}_{Al}^{O} = \frac{2N_{2O} + 3(N_O - N_{2O})}{N_O}. \tag{9}$$

This equation can be solved for $\bar{n}_{Al}^{O} = 4$ with $c_{Al}/c_O = 2(1-x)/(3-2x)$ to give $N_{2O}/N_O = (1+2x)/(3-2x)$ and $N_{3O}/N_O = 2(1-2x)/(3-2x)$. In the case when $x = 0.5$, $N_{2O}/N_O = 1$ so that no oxygen triclusters are present as found for crystalline $CaAl_2O_4$ and $BaAl_2O_4$.[25,26] In the case when $x = 0.4$, however, $N_{2O}/N_O = 9/11$ and $N_{3O}/N_O = 2/11$, i.e., 18.18% of the oxygen atoms will be threefold coordinated to Al atoms. In the case when $x = 1/3$, $N_{2O}/N_O = 5/7$ and $N_{3O}/N_O = 2/7$ as found for crystalline $CaAl_4O_7$.[30]

The mean number of triply coordinated oxygen atoms per $AlO_4$ tetrahedron $f_{tri}$ can also be estimated. The number of $AlO_4$ tetrahedra in the system is given by the number of Al atoms $N_{Al}$. From above, the number of threefold-coordinated oxygen atoms is given by $N_{3O} = 2N_O(1-2x)/(3-2x)$ and the number of associated tetrahedra is $3N_{3O}$. Since

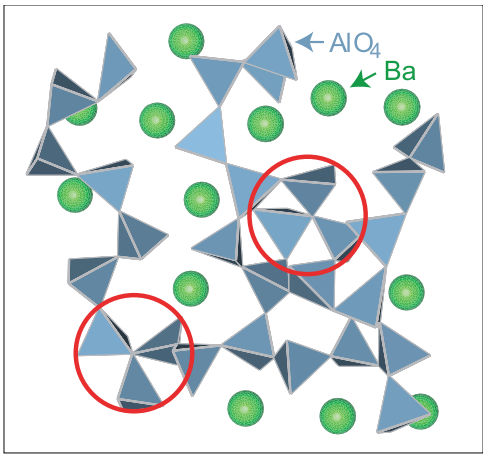


FIG. 7. (Color online) Slice through the model obtained for $(BaO)_{0.4}(Al_2O_3)_{0.6}$ glass from the RMC-I refinement, in which no coordination number constraints were applied, showing examples of oxygen triclusters (circled configurations) where a single oxygen atom is shared between three $AlO_4$ tetrahedra. The segment shown here corresponds to a box of area approximately 20 Å × 20 Å and depth 4 Å.

$N_O/N_{Al} = c_O/c_{Al}$, it follows that $f_{tri} = 3N_{3O}/N_{Al} = 3(1 - 2x)/(1 - x)$. Hence, $f_{tri} = 0$ if $x = 0.5$ or $f_{tri} = 1$ if $x = 0.4$. In the case when $x = 1/3$, $f_{tri} = 3/2$ as found for crystalline $CaAl_4O_7$ where half of the $AlO_4$ tetrahedra have one triply coordinated oxygen atom and the other half have two triply coordinated oxygen atoms.[30]

It is therefore interesting to investigate the connectivity of the network forming $AlO_4$ tetrahedra in the RMC-I refinement of the MD model for the $(BaO)_{0.4}(Al_2O_3)_{0.6}$ glass. In the RMC-I model, less than 3% of the oxygen atoms are isolated or nonbridging and the fractions of twofold- and threefold-coordinated oxygen atoms (as evaluated for a cutoff distance of 3.4 Å) are 76% and 21% where the majority of the latter (92%) are in triclusters. Thus, the fractions of twofold- and threefold-coordinated oxygen atoms are close to the values of 81.82% and 18.18%, respectively, which are predicted on the basis of Eq. (9). The results therefore support the presence of a high fraction of these overcoordinated oxygen sites, which are illustrated in Fig. 7. The Al-Al partial pair density function $d_{AlAl}(r)$ has two close first-neighbor peaks at $\simeq$2.8 and $\simeq$3.2 Å (Fig. 6), which integrate, using a cutoff distance of 3.8 Å, to give a coordination number $\bar{n}^{Al}_{Al} = 5.0$. For a corner-shared tetrahedral $AlO_4$ network in which $\bar{n}^{O}_{Al} = 4$ and $\bar{n}^{Al}_{O} = 2$, a coordination number $\bar{n}^{Al}_{Al} \simeq 4$ is expected.[62] The enhanced Al-Al coordination number for the barium aluminate glass is consistent with the proximity of a fifth tetrahedron due to oxygen tricluster formation. For example, in crystalline $CaAl_4O_7$, one half of the $AlO_4$ tetrahedra have a single triply coordinated oxygen atom and the nearest-neighbor Al-Al coordination number for these tetrahedra is five, as found by using a cutoff distance of 3.5 Å. In this crystal, the other half of the $AlO_4$ tetrahedra have two triply coordinated oxygen atoms and the nearest-neighbor Al-Al coordination number for these tetrahedra is six, i.e., the average nearest-neighbor Al-Al coordination number in crystalline $CaAl_4O_7$ is $\bar{n}^{Al}_{Al} = 5.5$.[30] These results suggest that most of the $AlO_4$ tetrahedra in $(BaO)_{0.4}(Al_2O_3)_{0.6}$ glass are associated with a single triply coordinated oxygen atom, in accordance with the predicted value of $f_{tri} = 1$ when $x = 0.4$.

In the spirit of the discussion leading to Eqs. (7)–(9), it is useful to compare the structure of the network formed by the Al and O atoms in $(BaO)_{0.4}(Al_2O_3)_{0.6}$ glass with the network formed in $GeO_2$ glass, an archetypal 2:1 binary network glass forming material for which an accurate set of partial structure factors has been measured by using the method of neutron diffraction with isotope substitution.[60,67] In both materials, the network is made predominantly from corner-shared $XO_4$ tetrahedra, where X denotes Al or Ge, and the Al-O and Ge-O bond distances are comparable at $\simeq$1.76 and 1.73 Å, respectively. The number density of the Al and O atoms in the $(BaO)_{0.4}(Al_2O_3)_{0.6}$ glass (0.0610 $Å^{-3}$) is comparable to the number density of $GeO_2$ glass (0.0629 $Å^{-3}$).[67] A comparison between the Faber-Ziman partial structure factors $S_{\alpha\beta}(Q)$ is made in Fig. 8. In this figure,

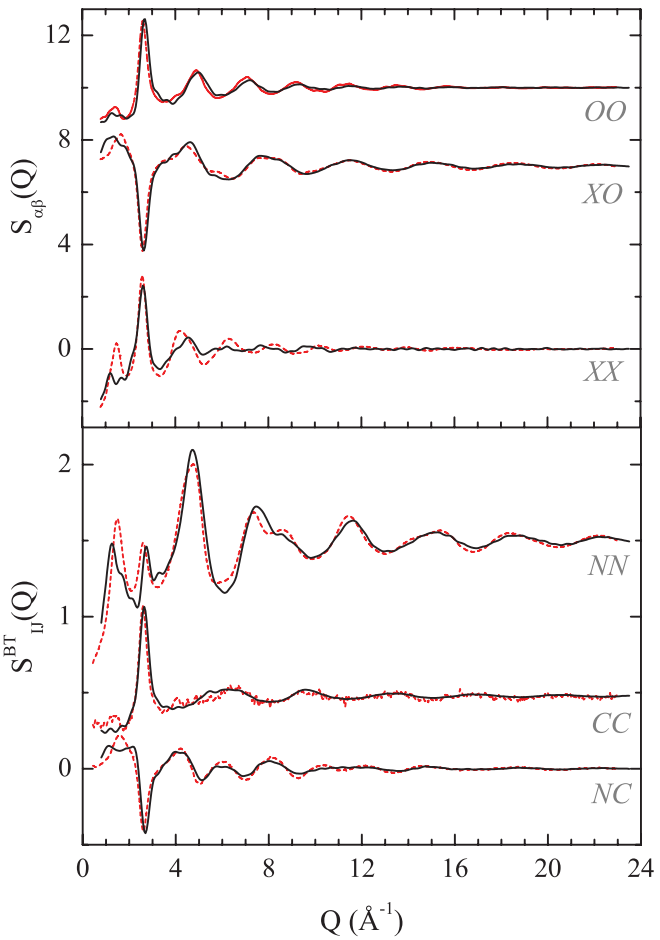


FIG. 8. (Color online) Comparison between the partial structure factors for (i) the network forming elements Al and O in $(BaO)_{0.4}(Al_2O_3)_{0.6}$ glass as obtained from the RMC-I refinement [solid dark (black) curves] and (ii) $GeO_2$ glass as obtained from experiment [light broken (red) curves] (Refs. 60 and 67). The upper panel shows the Faber-Ziman partial structure factors $S_{\alpha\beta}(Q)$, where X represents Al or Ge, and the lower panel shows their linear combination to give a representation of the Bhatia-Thornton partial structure factors $S^{BT}_{IJ}(Q)$ (see the text).

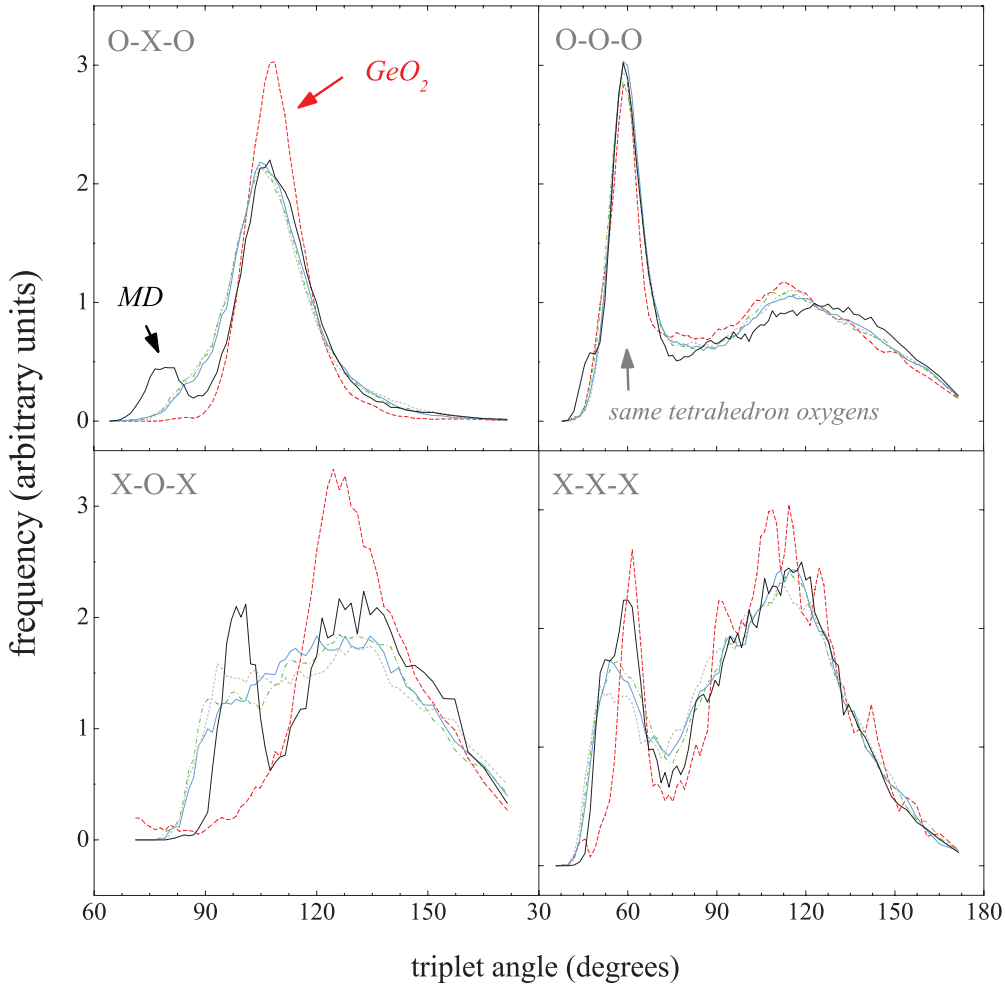


FIG. 9. (Color online) The bond-angle distributions for $(BaO)_{0.4}(Al_2O_3)_{0.6}$ glass as obtained from the MD simulation and from different RMC refinements of the MD structure. The solid dark (black) curves show the results obtained from the MD simulation, the solid light (blue) curves show the RMC-I results in which no coordination number constraints were applied, the broken (gray) curves show the RMC-II results in which the barium atoms were fixed in their initial positions, and the dotted (green) curves show the RMC-III results in which 100% of the aluminium atoms were constrained to be fourfold coordinated to oxygen. Also shown [broken light (red) curves] are the corresponding bond-angle distributions for a model of glassy $GeO_2$ (see the text). X denotes Al or Ge.

a comparison is also made between the Bhatia-Thornton number-number ($N$-$N$), number-concentration ($N$-$C$), and concentration-concentration ($C$-$C$) partial structure factors $S^{\mathrm{BT}}_{IJ}(Q)$, which describe the topological and chemical ordering in the glass and are defined by[68,69]

$$S^{\mathrm{BT}}_{N\text{-}N}(Q) = c_{\mathrm{X}}^2 S_{\mathrm{XX}}(Q) + c_{\mathrm{O}}^2 S_{\mathrm{OO}}(Q) + 2c_{\mathrm{X}}c_{\mathrm{O}}S_{\mathrm{XO}}(Q), \quad (10)$$

$$S^{\mathrm{BT}}_{C\text{-}C}(Q) = c_{\mathrm{X}}c_{\mathrm{O}}\{1 + c_{\mathrm{X}}c_{\mathrm{O}}[S_{\mathrm{XX}}(Q) + S_{\mathrm{OO}}(Q) - 2S_{\mathrm{XO}}(Q)]\}, \quad (11)$$

and

$$S^{\mathrm{BT}}_{N\text{-}C}(Q) = c_{\mathrm{X}}c_{\mathrm{O}}\{c_{\mathrm{X}}[S_{\mathrm{XX}}(Q) - S_{\mathrm{XO}}(Q)] - c_{\mathrm{O}}[S_{\mathrm{OO}}(A) - S_{\mathrm{XO}}(Q)]\}. \quad (12)$$

In the case of $(BaO)_{0.4}(Al_2O_3)_{0.6}$, the atomic fractions were evaluated by using Eqs. (7) and (8) such that $c_{\mathrm{Al}} = 6/17$ and $c_{\mathrm{O}} = 11/17$.

Figure 8 shows that there is a strong similarity between the $S_{\mathrm{OO}}(Q)$ and $S_{\mathrm{XO}}(Q)$ partial structure factors for the two glasses. The main difference is observed between the $S_{\mathrm{XX}}(Q)$ functions and, since these functions describe the correlations between the tetrahedron centers, this is related to different network connectivities as might be expected from the presence of oxygen triclusters in the aluminate glass. For example, the first sharp diffraction peak in $S_{\mathrm{XX}}(Q)$ at $\sim$1.6 Å$^{-1}$ is a signature of medium-range atomic ordering[70] and is a prominent feature for "strong" network glass-forming materials such as $GeO_2$. This feature is, however, shifted to smaller $Q$ and, as anticipated for a more "fragile" glass former,[67] it is much weaker in $S_{\mathrm{AlAl}}(Q)$. The damping of the oscillations at higher $Q$ in $S_{\mathrm{AlAl}}(Q)$ by comparison with $S_{\mathrm{GeGe}}(Q)$ is consistent with a greater distortion of the X-X correlations in the glass containing oxygen triclusters. The contrast in the topologies of the two networks is emphasized by the discrepancies observed between the Bhatia-Thornton number-number partial structure factors shown in Fig. 8.

A model for glassy $GeO_2$ was built from the available neutron diffraction data[60,67] by following a similar MD and

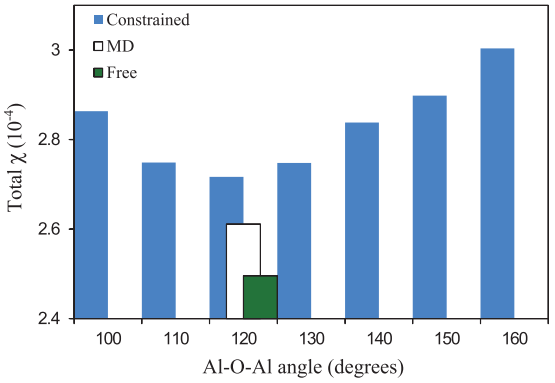


FIG. 10. (Color online) A comparison between the quality of fit parameter $\chi$ for various models of $(BaO)_{0.4}(Al_2O_3)_{0.6}$ glass and the principal intertetrahedral Al-O-Al bond angle corresponding to the peak position in the Al-O-Al bond-angle distribution. The $\chi$ parameter is defined such that $\chi^2 = \frac{1}{(2N)^2}\sum_i\{[S_N^{exp}(Q_i) - S_N^{mod}(Q_i)]^2 + [S_X^{exp}(Q_i) - S_X^{mod}(Q_i)]^2\}$, where superscripts denote the functions obtained either from experiment (exp) or from a model (mod) and the sum is over all of the $N$ discrete data points covering the range $0.5 \leqslant Q_i \leqslant 17.8$ Å$^{-1}$. The results obtained from the MD simulation (open histogram) and from the RMC-I refinement in which no coordination number constraints were applied [solid dark (green) histogram] are compared with the results obtained from RMC refinements in which the Al-O-Al bond angle was constrained to be at one of the specified values [solid light (blue) histograms].

RMC refinement procedure to that described in this paper. Several of the corresponding bond-angle distributions are shown in Fig. 9, where they are compared with the bond-angle distributions obtained from the MD and various RMC models of $(BaO)_{0.4}(Al_2O_3)_{0.6}$ glass. The X-O-X bond-angle distribution has a peak at 132° for $GeO_2$ as compared to 151° for $SiO_2$ (Ref. 71). For the aluminate glass, the MD simulation gives two peaks in the X-O-X bond-angle distribution, one at ∼125°, which is attributed to corner-sharing tetrahedra, and the other at ∼100°. The RMC refinements lead to a broadening of the latter, and the appearance of this feature is consistent with the formation of oxygen triclusters where, by comparison with twofold-coordinated oxygen atoms, the presence of a third tetrahedron "squeezes" the tetrahedra closer together.[29] The peak in the O-X-O bond-angle distribution at ∼80° in the MD simulation corresponds to fivefold-coordinated Al sites that disappear in the RMC refinement, leaving only the tetrahedral peak centered around 104°. However, this peak is noticeably broader than that observed for $GeO_2$, suggesting that the $AlO_4$ tetrahedra are more distorted.

To explore the sensitivity of the RMC-I model to the mean intertetrahedral Al-O-Al bond angle, refinements of the MD model were made in which this angle was fixed at various values between 100° and 160°. As shown in Fig. 10, the fit to the diffraction data obtained from refinement RMC-I, in which the Al-O-Al angle was unconstrained, is considerably better than the fits obtained from refinements in which the Al-O-Al angle was fixed. The results show a principal intertetrahedral angle of ∼120°, which is close to the limit noted in Ref. 72 for the transition from more open corner-shared tetrahedral networks to more tightly packed tetrahedral networks in which edge sharing begins to take place.

Oxygen triclusters have been detected by NMR heteronuclear correlation experiments between quadrupolar nuclei in $CaAl_2O_4$ glass, where they are present at the 5% level,[73] and they occur in crystalline $CaAl_4O_7$, where $N_{3O}/N_O = 2/7$.[30,31,66] Triclusters have also been found in a model of $(CaO)_{0.61}(Al_2O_3)_{0.39}$ glass constructed from a combination of MD, diffraction data and RMC methods where $N_{3O}/N_O = 5.9\%$,[23] and in an MD model of $(CaO)_{0.625}(Al_2O_3)_{0.375}$ glass where $N_{3O}/N_O \simeq 5\%$.[18] They have also been found in models of the liquid phase of $(CaO)_x(Al_2O_3)_{1-x}$ constructed from a combination of diffraction and MD methods. In the latter, the fraction of threefold-coordinated oxygen atoms was found to increase from 18% to 40% as the mole fraction of CaO was decreased from $x = 1/2$ to 1/3, but not all of these oxygen atoms are bound to three $AlO_4$ tetrahedra, i.e., other Al-centered polyhedra are present.[74] Threefold-coordinated oxygen atoms have been reported in glassy $(CaO)_{0.5}(Al_2O_3)_{0.5}$ under conditions of high pressure,[75] and oxygen triclusters form as a minor species in calcium aluminosilicate glasses.[23,65]

### B. Ba-O conformations

As discussed in Sec. VI A, in the RMC-I model, ≃21% of the oxygen atoms are triply coordinated in triclusters ($O_T$), ≃76% of the oxygen atoms are normal twofold-coordinated species ($O_N$), and very few of the oxygen atoms are isolated or nonbridging. Less than 9% of the Ba atoms are found to be connected to more than one $O_T$ atom and the average Ba-$O_T$ coordination number is small at $\bar{n}_{Ba}^{O_T} \simeq 0.5$. In contrast, the average Ba-$O_N$ coordination number is $\bar{n}_{Ba}^{O_N} \simeq 6.8$. The $Ba^{2+}$ ions therefore coordinate preferentially to the twofold-coordinated bridging oxygen atoms of the $AlO_4$ tetrahedra and avoid binding to oxygen atoms in triclusters. This is consistent with a squeezing together of the three $AlO_4$ tetrahedra around an $O_T$ atom, which inhibits a close approach of the large $Ba^{2+}$ ion. The barium ions appear to occupy voids in the network formed by the $AlO_4$ tetrahedra, and it is plausible that this offers an explanation for the wider glass-forming composition range for the calcium aluminate system, wherein the smaller radius of $Ca^{2+}$ versus $Ba^{2+}$ (1.00 Å versus 1.35 Å for a coordination number of six)[76] enables these ions to occupy the smaller voids in networks formed from corner-sharing $AlO_4$ tetrahedra. This aspect of glass formation in the alkaline-earth aluminate system warrants further investigation, and compounds incorporating the intermediate-sized $Sr^{2+}$ ion are therefore of interest.

## VII. CONCLUSIONS

The structure of $(BaO)_{0.4}(Al_2O_3)_{0.6}$ glass was investigated by neutron and x-ray diffraction, and a detailed atomistic model was made by using RMC to refine an initial MD model. This material is at an extreme limit of the glass-forming region in the barium aluminate system where there are insufficient oxygen atoms to form an ideal network of corner-shared $AlO_4$ tetrahedra in which the oxygen atoms are twofold coordinated. The results show that the system overcomes this oxygen

deficiency by forming a network of corner-shared $AlO_4$ tetrahedra in which $\simeq$21% of the oxygen atoms form triclusters. The $Ba^{2+}$ ions bind preferentially to the twofold-coordinated bridging oxygen atoms in the network structure, and not to the triclustered oxygen atoms, to give an average Ba-O coordination number $\bar{n}^{O}_{Ba} = 7.4$.


## ACKNOWLEDGMENTS

We would like to thank P. Palleau (ILL) for his assistance with the neutron diffraction experiment, A. Zeidler (Bath) for helpful comments on the manuscript, and the EPSRC for financial support. L.B. Skinner would also like to thank the EPSRC for a studentship, and also the US DOE for postdoctoral support (DE-FG02-09ER46650).



[1] S. R. Elliott, *Physics of Amorphous Materials*, 2nd ed. (Longman, Harlow, UK, 1990).

[2] A. Feltz, *Amorphous Inorganic Materials and Glasses* (VCH, Weinheim, 1993).

[3] M. Yamane and Y. Asahara, *Glasses for Photonics* (Cambridge University Press, Cambridge, UK, 2000).

[4] J. E. Shelby, J. Am. Ceram. Soc. **68**, 155 (1985).

[5] H. Hosono, K. Yamazaki, and Y. Abe, J. Am. Ceram. Soc. **68**, C304 (1985).

[6] L. D. Pye, in *Proceedings of the SPIE: Infrared Optical Materials* VI, edited by Solomon Musikant, Vol. 929 (Society of Photo-Optical Instrumentation Engineers (SPIE), Bellingham, WA, 1988), pp. 149–156.

[7] E. V. Uhlmann, M. C. Weinberg, N. J. Kreidl, and A. A. Goktas, J. Am. Ceram. Soc. **76**, 449 (1993).

[8] W. A. King and J. E. Shelby, Phys. Chem. Glasses **37**, 1 (1996).

[9] A. C. Hannon and J. M. Parker, J. Non-Cryst. Solids **274**, 102 (2000).

[10] J. P. Coutures, J. C. Rifflet, D. Billard, and P. Coutures, in *Proceedings of the Sixth European Symposium on Material Sciences under Microgravity Conditions*, Vol. ESA SP-256 (European Space Agency, Paris, 1987), pp. 427–430.

[11] M. C. Badets, C. Bessada, P. Simon, D. Billard, A. Douy, D. Massiot, J. C. Rifflet, F. Taulelle, and J. P. Coutures, in *Proceedings of the Seventh European Symposium on Materials and Fluid Sciences in Microgravity*, Vol. ESA SP-295 (European Space Agency, Paris, 1990), pp. 511–517.

[12] D. Massiot, D. Trumeau, B. Trouzo, I. Farnan, J.-C. Rifflet, A. Douy, and J.-P. Coutures, J. Phys. Chem. **99**, 16455 (1995).

[13] J. E. Shelby, C. M. Shaw, and M. S. Spess, J. Appl. Phys. **66**, 1149 (1989).

[14] L.-G. Hwa, C.-C. Chen, and S.-L. Hwang, Chin. J. Phys. (Taipei, Taiwan) **35**, 78 (1997).

[15] M. E. Lines, J. B. MacChesney, K. B. Lyons, A. J. Bruce, A. E. Miller, and K. Nassau, J. Non-Cryst. Solids **107**, 251 (1989).

[16] P. F. McMillan and B. Piriou, J. Non-Cryst. Solids **55**, 221 (1983).

[17] P. F. McMillan, W. T. Petuskey, B. Coté, D. Massiot, C. Landron, and J.-P. Coutures, J. Non-Cryst. Solids **195**, 261 (1996).

[18] B. W. M. Thomas, R. N. Mead, and G. Mountjoy, J. Phys.: Condens. Matter **18**, 4697 (2006).

[19] D. R. Neuville, L. Cormier, and D. Massiot, Chem. Geol. **229**, 173 (2006).

[20] D. R. Neuville, L. Cormier, V. Montouillout, and D. Massiot, J. Non-Cryst. Solids **353**, 180 (2007).

[21] C. J. Benmore, J. K. R. Weber, S. Sampath, J. Siewenie, J. Urquidi, and J. A. Tangeman, J. Phys.: Condens. Matter **15**, S2413 (2003).

[22] Q. Mei, C. J. Benmore, J. Siewenie, J. K. R. Weber, and M. Wilding, J. Phys.: Condens. Matter **20**, 245106 (2008).

[23] L. Cormier, D. Ghaleb, D. R. Neuville, J.-M. Delaye, and G. Calas, J. Non-Cryst. Solids **332**, 255 (2003).

[24] L. Hennet, I. Pozdnyakova, A. Bytchkov, D. L. Price, G. N. Greaves, M. Wilding, S. Fearn, C. M. Martin, D. Thiaudière, J.-F. Bérar, N. Boudet, and M.-L. Saboungi, J. Chem. Phys. **126**, 074906 (2007).

[25] W. Hörkner and H. K. Müller-Buschbaum, J. Inorg. Nucl. Chem. **38**, 983 (1976).

[26] S.-Y. Huang, R. Von Der Mühll, J. Ravez, J. P. Chaminade, P. Hagenmuller, and M. Couzi, J. Solid State Chem. **109**, 97 (1994).

[27] B. T. Poe, P. F. McMillan, B. Coté, D. Massiot, and J. P. Coutures, Science **259**, 786 (1993).

[28] D. R. Neuville, L. Cormier, A.-M. Flank, V. Briois, and D. Massiot, Chem. Geol. **213**, 153 (2004).

[29] E. D. Lacy, Phys. Chem. Glasses **4**, 234 (1963).

[30] D. W. Goodwin and A. J. Lindop, Acta Crystallogr. B **26**, 1230 (1970).

[31] V. I. Ponomarev, D. M. Kheiker, and N. V. Belov, Kristallografiya **15**, 1140 (1970) [Sov. Phys. Crystallogr. **15**, 995 (1971)].

[32] A. Utsunomiya, K. Tanaka, H. Morikawa, F. Marumo, and H. Kojima, J. Solid State Chem. **75**, 197 (1988).

[33] R. W. Nurse, J. H. Welch, and A. J. Majumdar, Trans. Brit. Ceramic Soc. **64**, 409 (1965).

[34] X. Ye, W. Zhuang, C. Deng, W. Yuan, and Z. Qiao, Comput. Coupling Phase Diagrams Thermochem. **30**, 349 (2006).

[35] B. Lazic, V. Kahlenberg, R. Kaindl, and A. Kremenović, Solid State Sci. **11**, 77 (2009).

[36] B. Frank and J. Liebertz, Glastechnische Berichte **41**, 253 (1968).

[37] N. Uchida, K. Uematsu, and K. Saito, J. Non-Cryst. Solids **134**, 176 (1991).

[38] C. C. Phifer, J. Non-Cryst. Solids **152**, 157 (1993).

[39] L. B. Skinner, A. C. Barnes, and W. Crichton, J. Phys.: Condens. Matter **18**, L407 (2006).

[40] R. L. McGreevy and L. Pusztai, Mol. Simul. **1**, 359 (1988).

[41] H. E. Fischer, A. C. Barnes, and P. S. Salmon, Rep. Prog. Phys. **69**, 233 (2006).

[42] H. Rauch and W. Waschkowski, in *Neutron Data Booklet*, 2nd ed., edited by A.-J. Dianoux and G. Lander (Old City Publishing, Philadelphia, 2003) , Chap. 1.1.

[43] E. N. Maslen, A. G. Fox, and M. A. O'Keefe, in *International Tables for Crystallography*, Vol. C, edited by A. J. C. Wilson (Kluwer Academic, Dordrecht, 1995), Chap. 6.1.1, p. 476.

[44] D. T. Cromer, J. Appl. Cryst. **16**, 437 (1983).

[45] A. Zeidler, J. W. E. Drewitt, P. S. Salmon, A. C. Barnes, W. A. Crichton, S. Klotz, H. E. Fischer, C. J. Benmore, S. Ramos, and A. C. Hannon, J. Phys.: Condens. Matter **21**, 474217 (2009).

[46] J. K. R. Weber, J. J. Felten, and P. C. Nordine, Rev. Sci. Instrum. **67**, 522 (1996).

[47] *Handbook of Chemistry and Physics*, 72nd ed., edited by D. R. Lide (Chemical Rubber Company Press, Boca Raton, 1991).
[48] A. C. Barnes, L. B. Skinner, P. S. Salmon, A. Bytchkov, I. Pozdnyakova, T. O. Farmer, and H. E. Fischer, Phys. Rev. Lett. **103**, 225702 (2009).
[49] H. E. Fischer, G. J. Cuello, P. Palleau, D. Feltin, A. C. Barnes, Y. S. Badyal, and J. M. Simonson, Appl. Phys. A **74**, S160 (2002).
[50] J. Zaleski, G. Wu, and P. Coppens, J. Appl. Cryst. **31**, 302 (1998).
[51] A. P. Hammersley, ESRF Report No. ESRF97HA02T, European Synchrotron Radiation Facility, Grenoble, France, 1997.
[52] W. Smith and T. R. Forester, J. Mol. Graphics **14**, 136 (1996).
[53] W. Smith, T. R. Forester, I. T. Todorov, and M. Leslie, *The DL_POLY_2 User Manual* (CCLRC Daresbury Laboratory, Daresbury, UK, 2006), v2.16.
[54] T. S. Bush, J. D. Gale, C. R. A. Catlow, and P. D. Battle, J. Mater. Chem. **4**, 831 (1994).
[55] E. Lorch, J. Phys. C: Solid State Phys. **2**, 229 (1969).
[56] R. A. Martin, P. S. Salmon, D. L. Carroll, M. E. Smith, and A. C. Hannon, J. Phys.: Condens. Matter **20**, 115204 (2008).
[57] E.-T. Kang, S.-J. Lee, and A. C. Hannon, J. Non-Cryst. Solids **352**, 725 (2006).
[58] M. C. Eckersley, P. H. Gaskell, A. C. Barnes, and P. Chieux, Nature (London) **335**, 525 (1988).
[59] P. H. Gaskell, M. C. Eckersley, A. C. Barnes, and P. Chieux, Nature (London) **350**, 675 (1991).
[60] P. S. Salmon, A. C. Barnes, R. A. Martin, and G. J. Cuello, J. Phys.: Condens. Matter **19**, 415110 (2007).
[61] I. Petri, P. S. Salmon, and H. E. Fischer, Phys. Rev. Lett. **84**, 2413 (2000).
[62] P. S. Salmon, J. Phys.: Condens. Matter **19**, 455208 (2007).
[63] G. N. Greaves and S. Sen, Adv. Phys. **56**, 1 (2007).
[64] L. B. Skinner, A. C. Barnes, P. S. Salmon, and W. A. Crichton, J. Phys.: Condens. Matter **20**, 205103 (2008).
[65] J. F. Stebbins and Z. Xu, Nature (London) **390**, 60 (1997).
[66] J. F. Stebbins, J. V. Oglesby, and S. Kroeker, Am. Mineralogist **86**, 1307 (2001).
[67] P. S. Salmon, A. C. Barnes, R. A. Martin, and G. J. Cuello, Phys. Rev. Lett. **96**, 235502 (2006).
[68] A. B. Bhatia and D. E. Thornton, Phys. Rev. B **2**, 3004 (1970).
[69] P. S. Salmon, Proc. R. Soc. London, Ser. A **437**, 591 (1992).
[70] P. S. Salmon, Proc. R. Soc. London, Ser. A **445**, 351 (1994).
[71] M. G. Tucker, D. A. Keen, M. T. Dove, and K. Trachenko, J. Phys.: Condens. Matter **17**, S67 (2005).
[72] M. Wilson and P. S. Salmon, Phys. Rev. Lett. **103**, 157801 (2009).
[73] D. Iuga, C. Morais, Z. Gan, D. R. Neuville, L. Cormier, and D. Massiot, J. Am. Chem. Soc. **127**, 11540 (2005).
[74] J. W. E. Drewitt, S. Jahn, V. Cristiglio, A. Bytchkov, M. Leydier, S. Brassamin, H. E. Fischer, and L. Hennet, J. Phys.: Condens. Matter **23**, 155101 (2011).
[75] I. Daniel, P. F. McMillan, P. Gillet, and B. T. Poe, Chem. Geol. **128**, 5 (1996).
[76] U. Müller, *Inorganic Structural Chemistry* (Wiley, Chichester, 1993).